DEPARTMENT OF PHYSICS

UNIVERSITY OF JYVÄSKYLÄ

Master's thesis

TESTING OF LASER ABLATION ION SOURCE FOR JYFLTRAP

BY

KATERYNA POLESHCHUK

Supervisor: Veli Kolhinen

UNIVERSITY OF JYVÄSKYLÄ

Jyväskylä, Finland

August 2015

Abstract

In this work, we have constructed and tested a laser ablation ion source for JYFLTRAP Penning trap at the IGISOL (Ion Guide Isotope Separator On-line) facility. The calibration of the Penning trap parameters requires reference ions or ion clusters that have well-known masses with relatively small mass uncertainty. These ions and ion clusters can be created with certain solid targets, which contain large amounts of isotopes of reference masses and by using a laser for target ablation. In this work simulations of ion source parameters, construction, testing and improving a laser ablation ion source setup have been done. Targets with relatively large abundances of ^{63}Cu and ^{65}Cu, ^{85}Rb, ^{87}Rb, ^{115}In, ^{120}Sn have been used for the laser ablation. Some of these ions were successfully created and measured with the Penning trap.

CONTENTS

LIST OF TABLES

LIST OF FIGURES

1.   Introduction

The JYFLTRAP Penning trap is a double cylindrical trap structure [1, 2] and it has been constructed for precise mass measurements at IGISOL [3]. The main components of IGISOL area are shown in Fig. 1.1. JYFLTRAP is also used for isobaric purification of radioactive ion beams of short-lived exotic isotopes. The Penning trap at IGISOL is playing an important role in mass measurements related to astrophysical studies, investigation of nuclei structure with post-trap spectroscopy and etc.

Isotopes produced in fission reactions are delivered to the Penning trap through an RFQ cooler/buncher [4], where the beam of short-lived exotic isotopes reduces its emittance and energy spread. Later on, cooled and bunched ions are injected into the first, purification Penning trap where ion bunch is purified by applying a mass-selective buffer gas-cooling technique [5]. This technique is capable of purifying the ions of interest even from its isobars. After the purification, the ions are transported to the second Penning trap, where mass measurements are performed. The ions released from the second Penning trap are detected with a chevron type microchannel plate (MCP) detector or they are transported further to subsequent spectroscopy setups.

Both Penning traps of JYFLTRAP are placed in a highly homogeneous magnetic field, created by 7 T superconducting solenoid. To be able to measure the strength of magnetic field B cross-reference mass measurements of nuclei with well-known masses are required. These measurements are based on the determination of the cyclotron frequency of ions

$$f_c = \frac{1}{2\pi} \frac{qB}{m} \tag{1.1}$$

where B is the magnetic field, q is the charge state of the ion and m is the mass of the ion. Hence, by determining the cyclotron frequency of an isotope with a

well-known mass one can determine the magnetic field. Therefore, after this, the determination the cyclotron frequency of an ion that has unknown mass one obtains also the mass of that ion.

In order to obtain ions that have well-known masses, a laser ablation ion source was built. By using this ion source, we were able to produce such nuclei as ^{85}Rb, ^{87}Rb, ^{115}In which have mass uncertainties of the order of 10 eV. These nuclei were used in test measurements which would allow determining the magnetic field with a high accuracy relying on the cyclotron frequency on which they circulate in the magnetic field of JYFLTRAP.
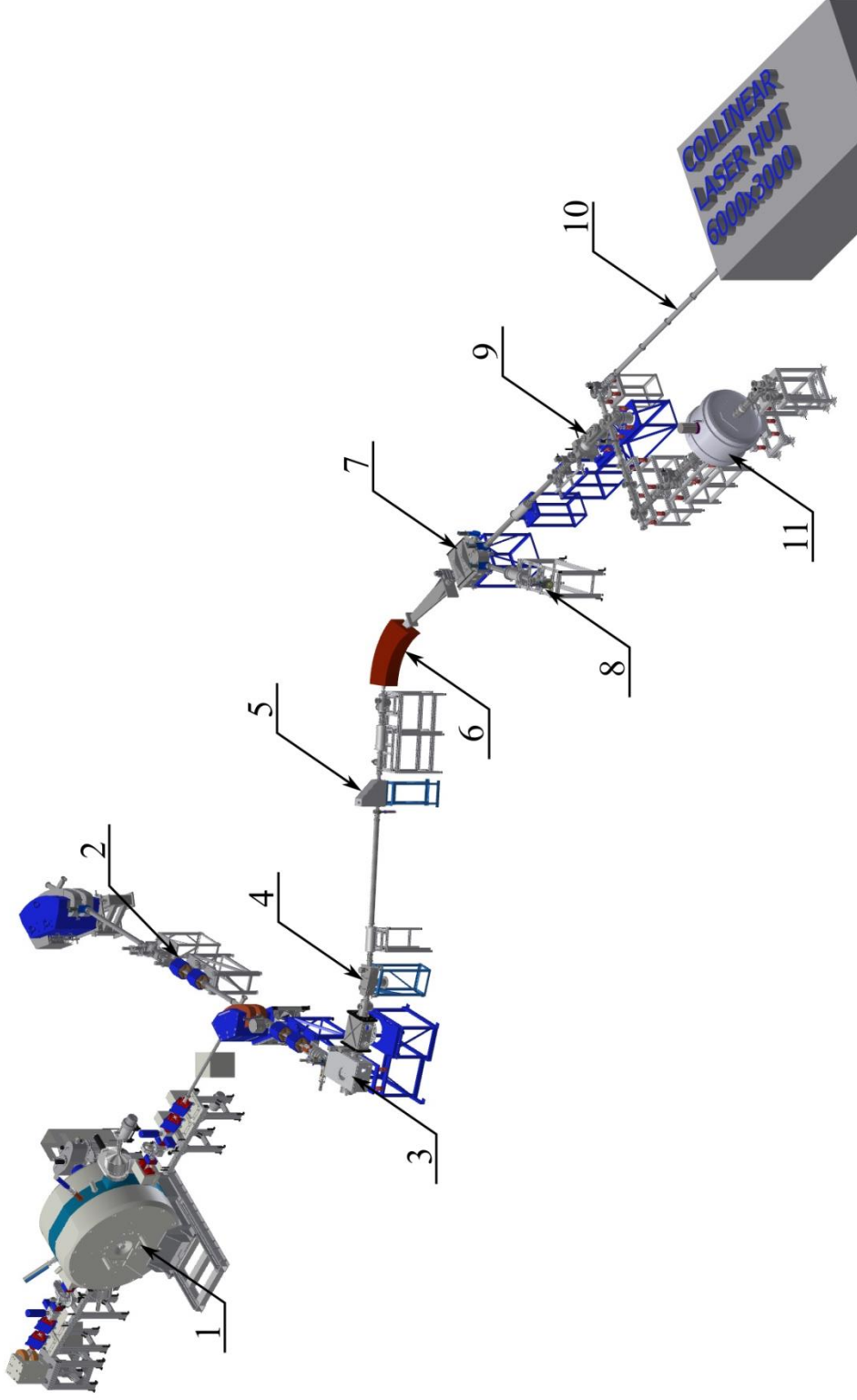
Fig. 1.1: General picture of the IGISOL laboratory showing. 1) high current MCC30/15 light ion cyclotron, 2) K130 cyclotron beam line, 3) target chamber, 4) 15° bender, 5) 90° bender with vertical line, 6) 55° dipole magnet M/ΔM≈500, 7) electrostatic beam switchyard, 8) spectroscopy line, 9) RFQ cooler/buncher, 10) collinear laser spectroscopy line, 11) Penning traps.

2.   The principle of IGISOL and the JYFLTRAP setup

2.1.   MCC-30/15 cyclotron at IGISOL

The cyclotron is designed for acceleration negative hydrogen ions H$^-$ up to 30 MeV energy with a beam current up to 100 µA and negative deuterium ions D$^-$ up to 15 MeV energy with a beam current up to 50 µA [6].

This cyclotron is equipped with external beam injection, which was created on basis of multicusp source, and two extraction systems for the beam transportation to the distant targets. These extraction systems can extract the protons in the range from 18 MeV to 30 MeV and deuteriums in the range between 9 MeV and 15 MeV in the opposite directions. A general view of the cyclotron MCC-30/15 is shown in Fig. 2.1.
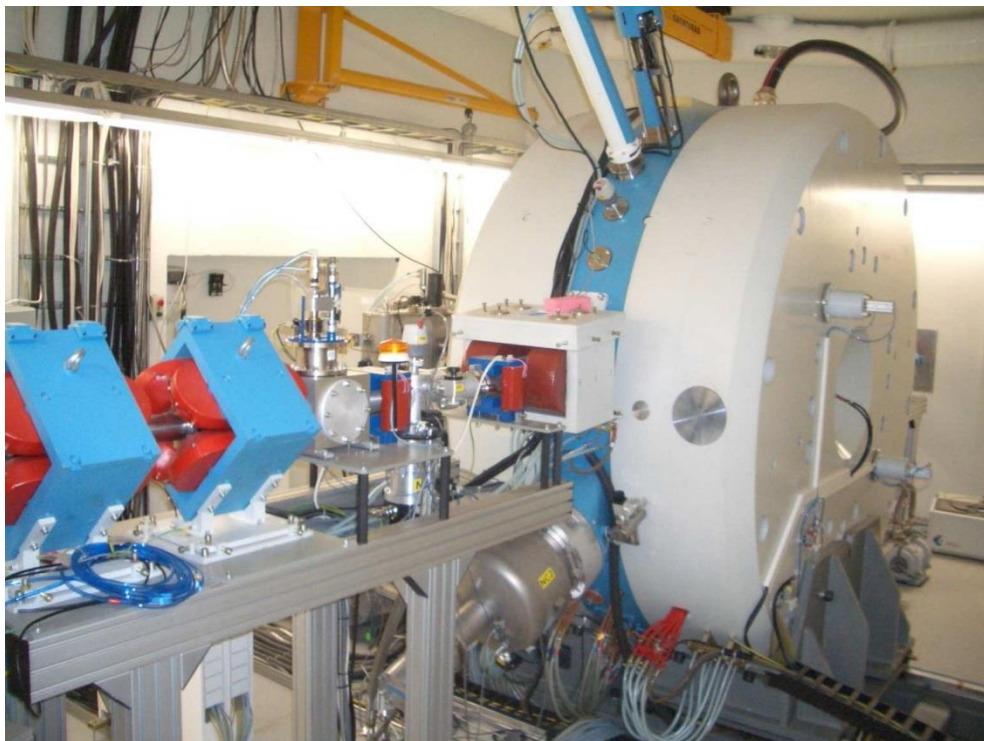
Fig. 2.1: A general view of the cyclotron MCC-30/15.

2.2. Principle of the IGISOL method

At IGISOL facility, one can produce and mass separate a wide range of short-lived ion beams of exotic nuclei that play an important role in studies of fundamental nuclear properties. A detailed description of IGISOL-4 facility can be found in [7, 8]. The primary ion beam can be delivered either from the light-ion MCC-30/15 or from the K-130 cyclotron to the IGISOL target chamber. The interaction of the primary beams with a target leads to a proton-induced fission reaction. Typically ^{238}U target is used. Alternatively a light/heavy ion fusion evaporation reaction is used depending on the desired reaction product. The products formed in the reaction are thermalized in the helium gas in the ion-guide. The schematic view of the IGISOL method is presented in Fig. 2.2.
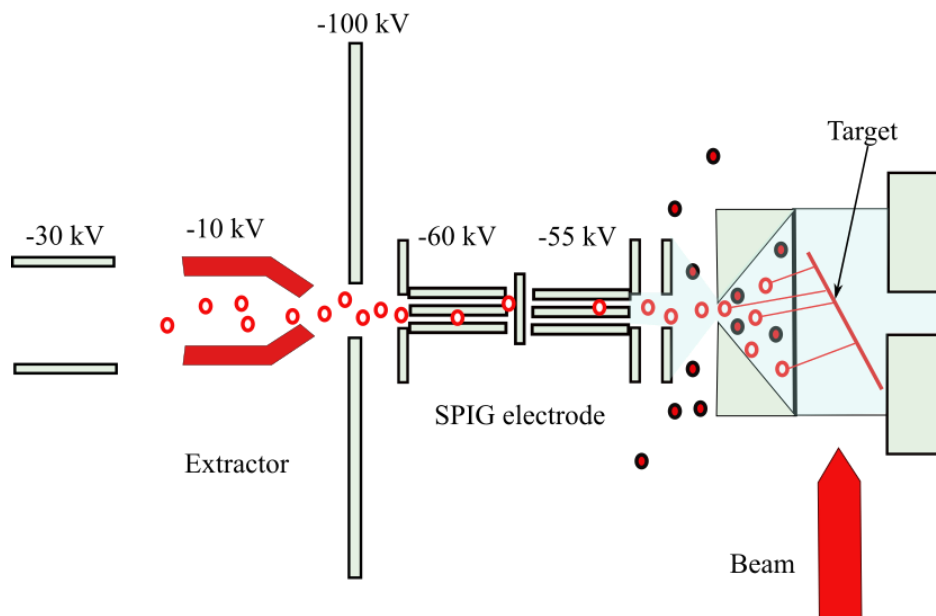
Fig. 2.2: A schematic design of an ion-guide.

During this process some part of the reaction products obtains +1 charge state. The reaction products are guided further with a gas flow and with a sextupole ion-guide (SPIG) [9, 10] into a different pumping stage and accelerated up to 30q keV energy, where q is the charge state of the ion, i.e. singly-charged ions get 30 keV energy.

2.3. JYFLTRAP

JYFLTRAP consists of a radiofrequency quadrupole (RFQ) cooler/buncher [4] and two cylindrical Penning traps inside the superconducting solenoid (7 T). Fig. 2.3 shows the photo of the JYFLTRAP area. The photos of the RFQ cooler/buncher structure and the superconducting solenoid of the JYFLTRAP Penning trap are represented in Figs. 2.4 and 2.5, respectively.
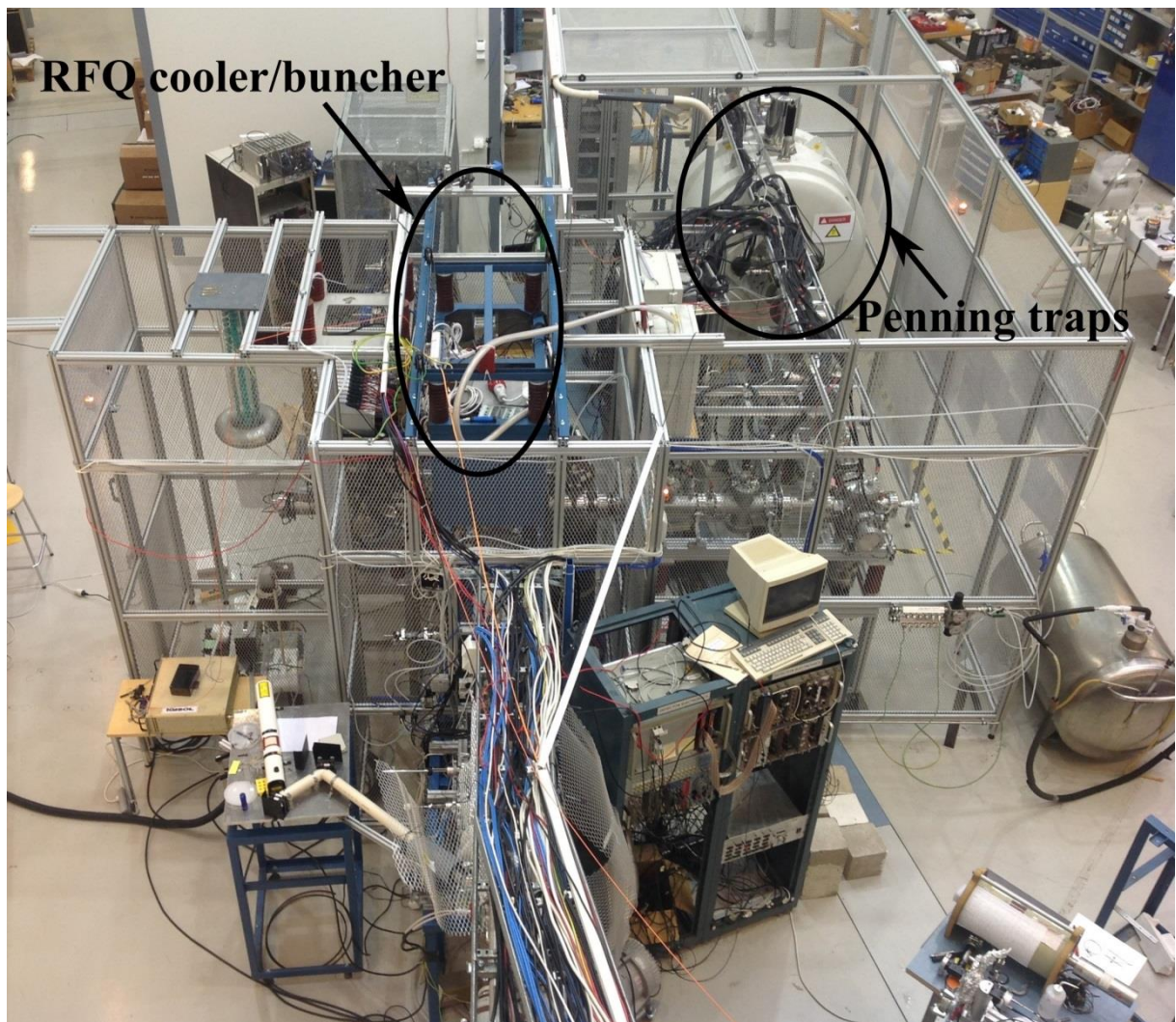
Fig. 2.3: View of the JYFLTRAP area at the IGISOL hall.

Fig. 2.4: The RFQ structure taken out from the vacuum chamber.

Fig. 2.5: The superconducting solenoid of the JYFLTRAP Penning trap.

2.3.1 Radiofrequency quadrupole cooler/buncher

The radiofrequency quadrupole (RFQ) cooler/buncher is designed for decreasing the emittance and the energy spread of a continuous beam coming from IGISOL. The RFQ device can be operated either in a way that it gives continuous beam through or in a bunching mode. The latter is required when guiding ions into the Penning traps.

The RFQ device is at high-voltage platform and the beam is decelerated down to few 100 eV before it goes into the volume filled with the buffer gas (helium) with pressure in the range of 0,01 and 0,1 mbar.

The RFQ structure consists on four rods where the radiofrequency voltage is applied for keeping ions trapped in the radial direction. The rods are divided in the segments for creating a DC slope and the potential minimum for the bunching of the ions. The ions collide with the He atoms of the buffer gas and they lose their kinetic energy, and are collected in the potential minimum. Then after decreasing the voltage on the last rod segments an ion bunch is extracted from the RFQ structure. Fig. 2.6 illustrates this principle.
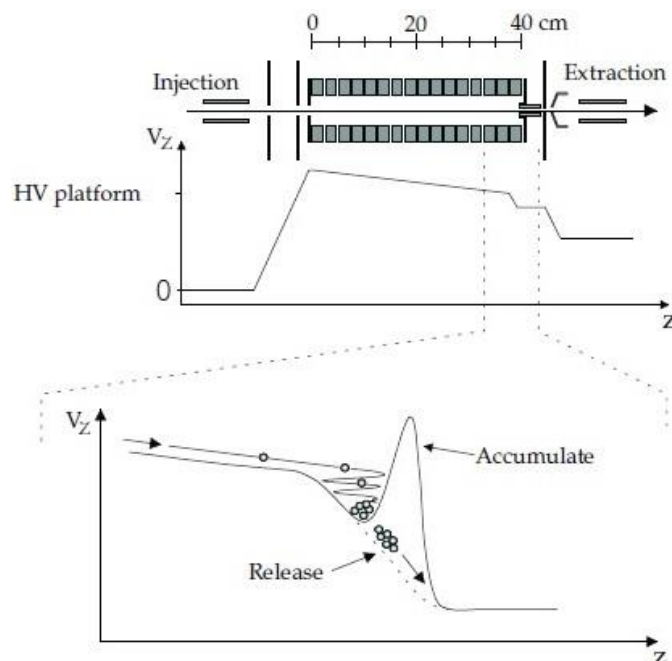
Fig. 2.6: A schematic picture of the RFQ cooler/buncher.

The ion bunch released from the gas-filled RFQ is typically $10 - 20$ μs long and has energy spread of the order of 1 eV.

2.3.2. Ion motions in the Penning traps

A Penning trap consists of an electric field and a parallel magnetic field and it is used for holding charged particles or charged particles clouds in a small volume. Such traps are enabling the investigation of isolated particles during sufficiently long time and thereby give a possibility to measure some of the properties of trapped ions.

Fig. 2.7 demonstrates two different types of Penning trap consisting of two end caps and a ring electrode.
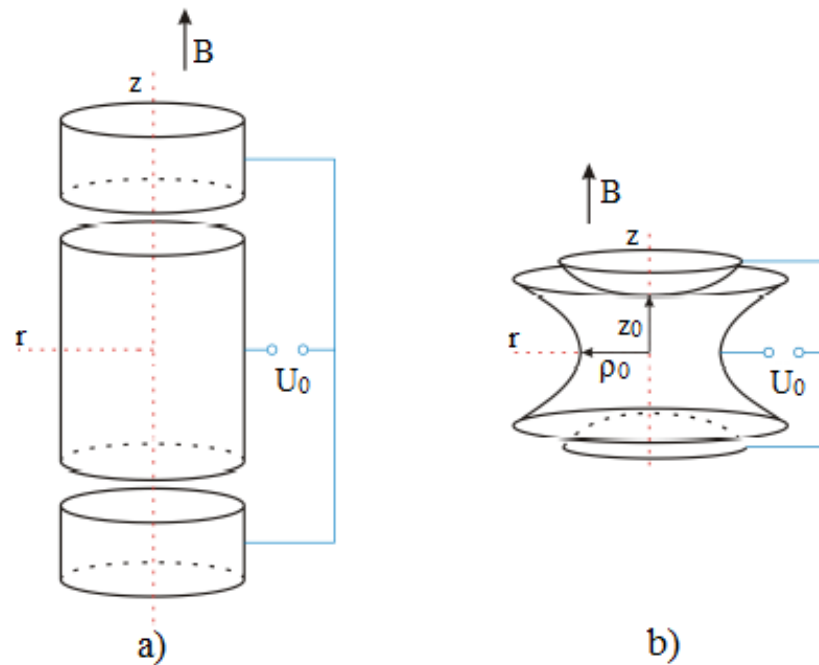
Fig. 2.7: Structures of a cylindrical (a) and a hyperbolic (b) traps. The ring electrode is the in middle and the end caps are on top and below of it.

For capturing positive (negative) particles a positive (negative) voltage relative to the central ring is applied to the end caps. Aim is to create the following potential

$$U(\rho,z) = \frac{U_0}{4d^2}(\rho^2 - 2z^2). \qquad (2.1)$$

This can be done either by electrode shapes or using cylindrical rings with a certain length to diameter ratio. Here U_0 is a potential difference between the ring electrodes and the end caps, ρ_0 and z_0 are distance between the center of the ring electrode and the inner surface of the ring electrode and end caps, respectively, and

$$d = \sqrt{2z_0^2 + \rho_0^2} \qquad (2.2)$$

is characteristics trap parameter defined by the size of the trap.

The axial magnetic field traps the particles in a horizontal plane. A trajectory of motion of an ion in horizontal plane is just circulation. But when one adds there the electric field required to trap the ions in the axial direction the ion motion gets more complicated. This trajectory includes two rotations with different radii and frequencies, herewith center of one circle moves along other circle see Fig.2.8.
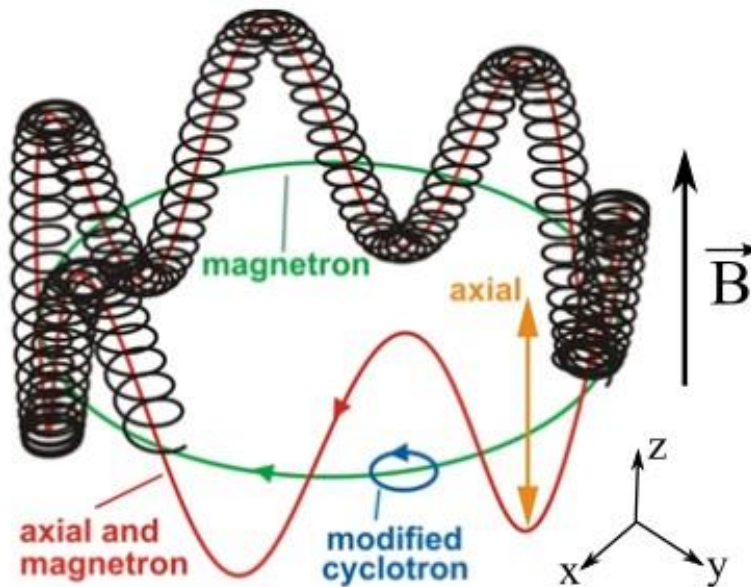
Fig. 2.8: Trajectory of a motion of one ion in a Penning trap. The motion consists of three different independent movements: an axial oscillation and two radial motions which are called magnetron and modified cyclotron motions.

The cyclotron frequency for a particle with the mass m and the charge q in the magnetic field B is equal

$$\omega_c = q\frac{B}{m}. \qquad (2.3)$$

The frequency of the harmonic oscillations of the particle along z-axis is

$$\omega_z = \sqrt{\frac{qU}{md^2}} \qquad (2.4)$$

where q is the charge of the ion, U is the potential difference, ω_c is the cyclotron frequency, ω_z is the frequency of harmonic oscillations of particle along the z-axis and d is the characteristics trap parameter defined by the size of the trap.

The two radial motions are the magnetron motion with the frequency of ω_- and the modified cyclotron motion with the frequency of ω_+, where

$$\omega_- = \frac{\omega_c}{2} - \sqrt{\frac{\omega_c^2}{4} - \frac{\omega_z^2}{2}}, \qquad (2.5)$$

$$\omega_+ = \frac{\omega_c}{2} + \sqrt{\frac{\omega_c^2}{4} - \frac{\omega_z^2}{2}}. \qquad (2.6)$$

In an ideal trap, these two frequencies sum up to the true cyclotron frequency [11].

$$\omega_c = \omega_+ + \omega_-. \qquad (2.7)$$

2.3.3 Penning traps of JYFLTRAP

After the RFQ cooler/buncher device ions are transported towards the Penning traps. Two cylindrical Penning traps are inside the superconducting solenoid (7 T). These traps are separated by a diaphragm with a diameter of 1.5 mm. The first trap is used for the isobaric purification of the ion bunch in the buffer gas. The second trap which is operated in the ultra-high vacuum is used for the precision mass measurements. Both traps consist of end caps, ring electrodes

and two correction electrodes at both sides between the ring and the end cap electrodes. The first correction electrodes which are closest to the ring electrode are divided into two segments. The ring electrodes are separated on eight segments in order to be able to generate an RF field for the dipole and the quadrupole excitations [1]. Figs. 2.9 and 2.10 show the electrode structure of JYFLTRAP. An overview of the setup is shown in Fig. 2.11 displaying the schematic layout.
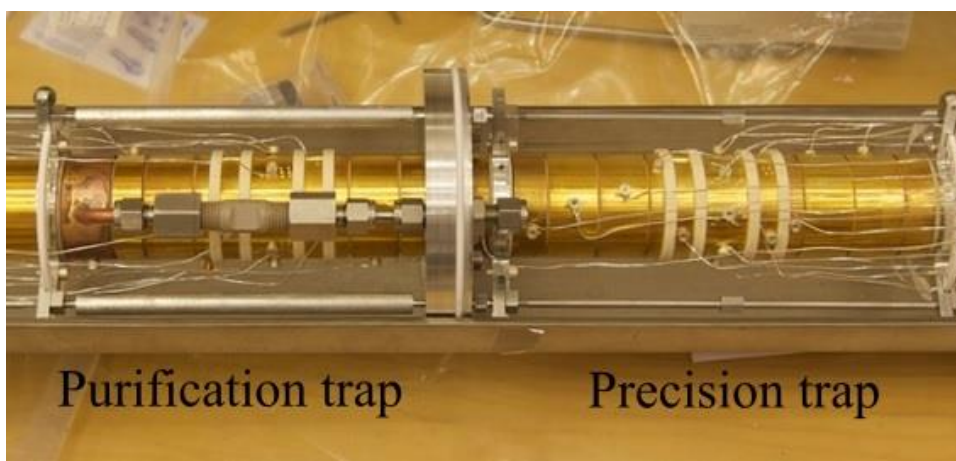
Fig. 2.9: A photo of the purification and the precision traps electrodes.
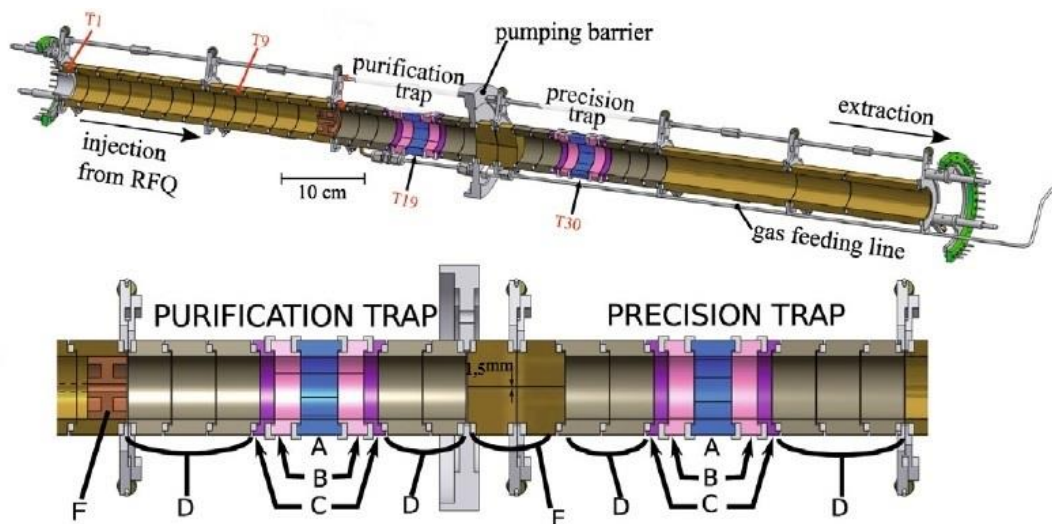
Fig. 2.10: The electrode structure of JYFLTRAP. In the upper picture the trap electrodes from left to right are marked T1, T2 and so on. The ring electrodes are T19 and T30. In the lower picture A are the 8-fold split ring electrodes, B are the 2-fold split inner correction electrodes, C is outer correction ring and D are end cap electrodes. E and F are the electrodes restricting the gas flow out.
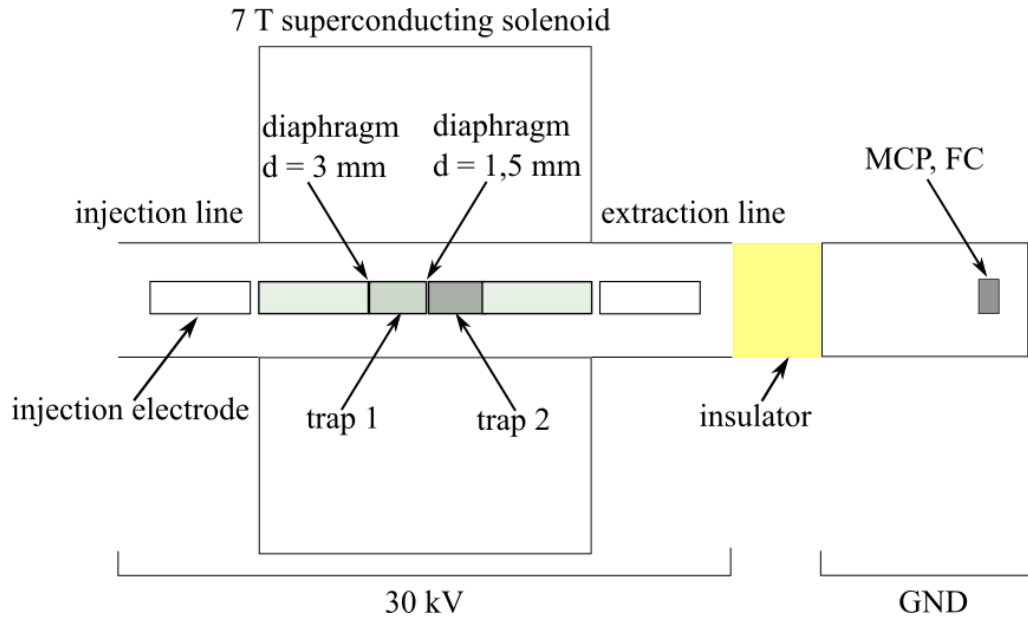
Fig. 2.11: A schematic view of the JYFLTRAP system (side view).

2.3.4 Purification trap

The first trap of the double trap system is the purification trap. This trap is filled with the buffer gas (helium) with a pressure of 10^{-4} mbar. By decreasing and increasing of voltage of the end cap of purification trap ions are injected and captured inside the trap. In the purification trap ions lose the axial energy when they collide with the buffer gas atoms. The time required in this process is such that the axial oscillation of ions is minimized and they are located in the center of trap, this is done usually in 50-100 ms at 10^{-4} mbar gas pressure. After the axial cooling a dipole RF excitation is applied to the segments of the ring electrode at magnetron frequency. In this excitation one applies the same amplitude, but the opposite phase in two opposite segments of the ring electrode. The dipole configuration of ring electrodes is given in Fig. 2.12 (a).
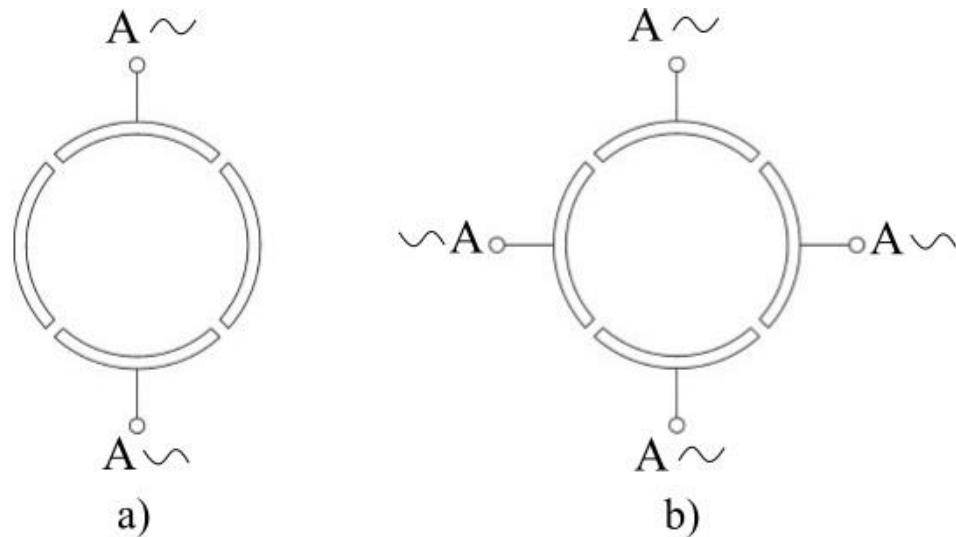
Fig. 2.12: The ring electrode structure of the Penning trap a) dipole configuration and b) quadrupole configuration.

This RF field moves all ions captured in the trap away from the trap center to larger orbits. And when ejected through a narrow channel this results in a decrease of the ion count rate as visible in Fig.2.13, if appropriate frequency and amplitude are found. For JYFLTRAP the magnetron frequency is 1740 Hz [12].
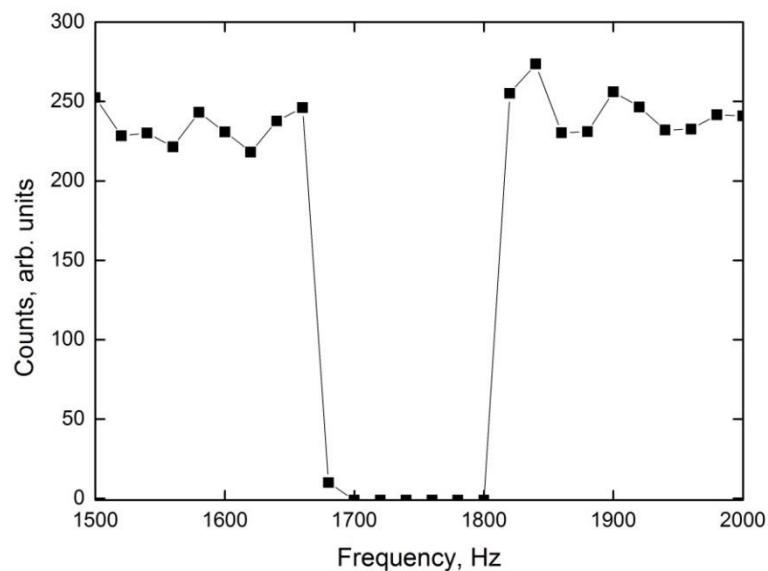
Fig. 2.13: Frequency scan for dipole excitation to determine the magnetron frequency. This excitation removes all ions from the trap center, so that they are not ejected from the trap.

A quadrupole radiofrequency excitation is used for coupling of the magnetron and the modified cyclotron motions. In this excitation one applies the same

amplitude and the phase to the opposite segments and the same amplitude and opposite phase to the neighboring segments, see Fig. 2.12 (b). The magnetron motion turns into the modified cyclotron motion by using a quadrupole excitation with a frequency, which corresponds to the cyclotron frequency of a certain mass. Herewith, while the magnetron radius decreases, the radius of modified cyclotron motion increases, what is shown in Fig. 2.14.
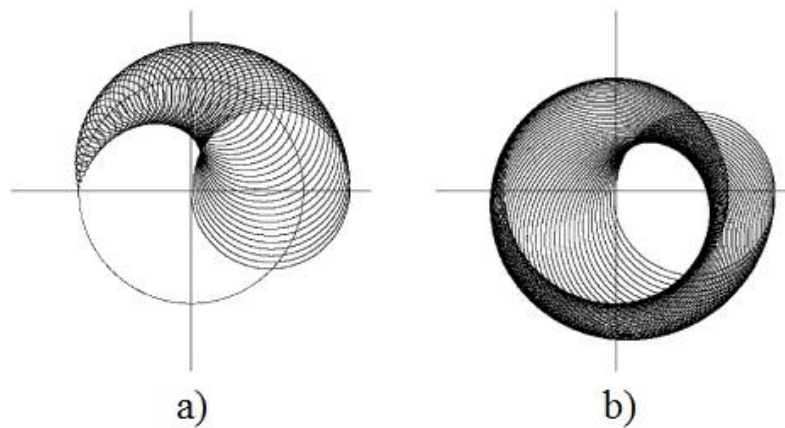
Fig. 2.14: The conversion of the magnetron motion into the modified cyclotron motion in quadrupole excitation at the resonance frequency a) in the first half and b) in the second half.

If one applies a quadrupole excitation at cyclotron frequency of trapped ions of the mass m and the charge state q in the magnetic field B

$$f_c = \frac{1}{2\pi} \frac{qB}{m} \tag{2.8}$$

in the purification trap, it will recenter those ions back to the center of the trap.

The trajectory of ion motion in the buffer gas with the quadrupole excitation is shown in the Fig. 2.15 (b). The purification trap is used mainly for the beam purification, but it can be used too for mass measurements in a form of the dependence of number of counts on the cyclotron frequency. Fig. 2.16 shows an example of a frequency scan.
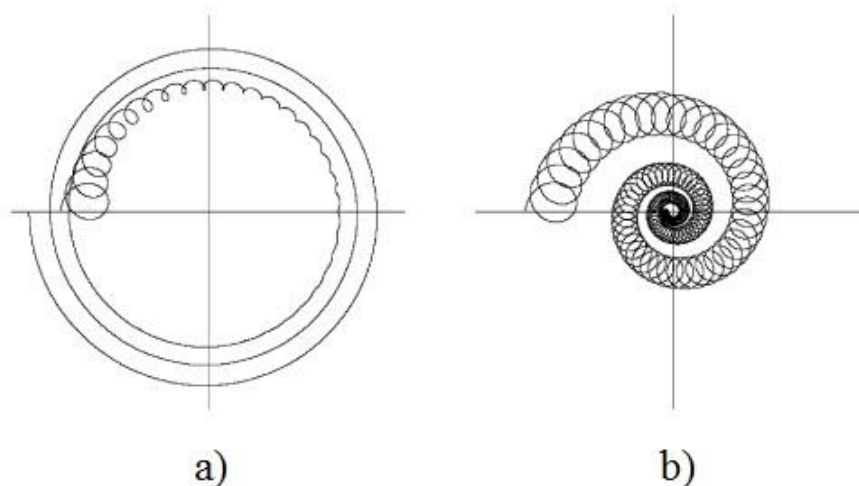
Fig. 2.15: The ion motion in the purification trap a) without quadrupole excitation and b) with quadrupole excitation at cyclotron frequency.
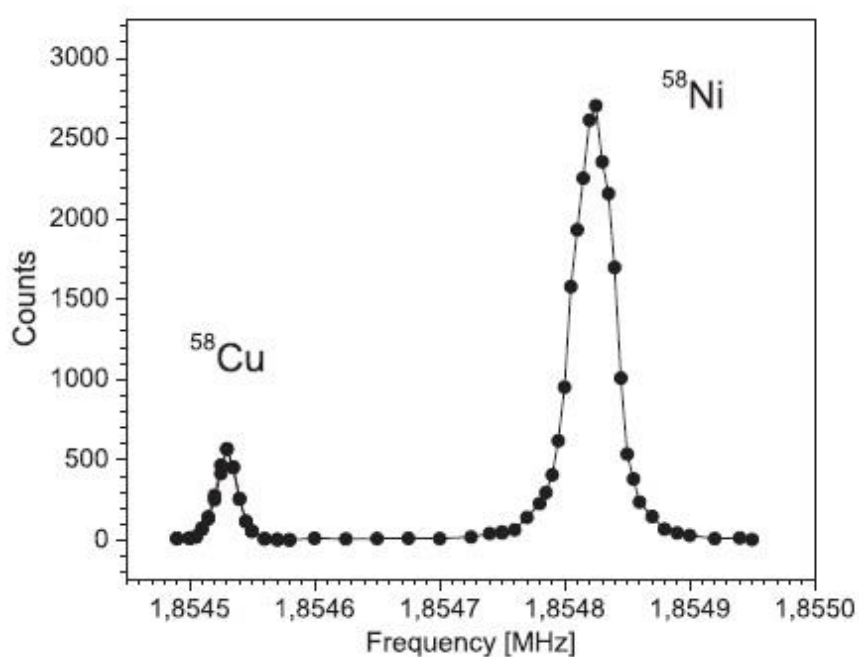
Fig. 2.16: Frequency scan of a quadrupole excitation for ^{58}Ni and ^{58}Cu. The solid line is a Gaussian fit to the data, which has been added to guide the eye.

By varying of the amplitude, the excitation times and the buffer gas pressure, the resolving power can be improved. The resolution of the purification process is 20 – 100 Hz, which is equivalent to $M/\Delta M = 10^4 – 10^6$.

2.3.5 Precision trap

After the purification trap, cooled and centered ions with a certain charge-to-mass ratio are transported into the precision trap. This is done by lowering the voltages of the electrodes that are between the traps. The precision trap is used for mass measurement and it is operated in high vacuum. In this trap the cyclotron frequency of the ions is determined by using the time-of-flight ion-cyclotron resonance (TOF-ICR) technique [13].

This method is based on conversion of the magnetron motion into the modified cyclotron motion by applying a quadrupolar RF field. After one conversion to the modified cyclotron motion the radial energy of the ions is at maximum. When ions are extracted into the drift section, where the magnetic field $\vec{B}$ changes, the radial energy of ions resulting in a stronger acceleration, see Fig. 2.17. The gradient force $\vec{F}$ is proportional to the orbital magnetic moment $\vec{\mu}$

$$\vec{\mu} = \frac{E_r}{B}\hat{z} \tag{2.9}$$

and therefore to the radial energy E_r

$$\vec{F} = -\vec{\mu}(\vec{\nabla}\vec{B}) = -\frac{E_r}{B} \cdot \frac{\partial B_z}{\partial z}\hat{z} \tag{2.10}$$

This finally leads to a shorter flight time from the trap to the detector, which is located outside the magnet and the arrival time relative to the trap opening time is registered.
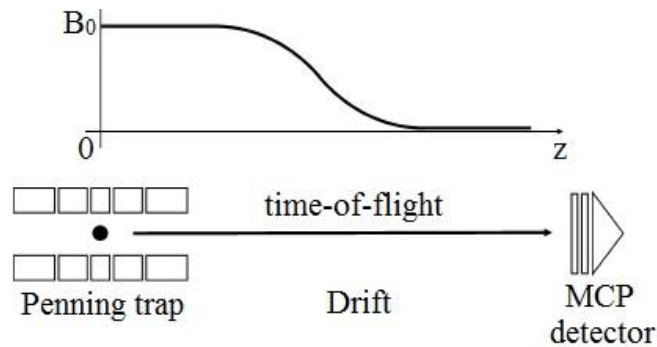
Fig. 2.17: Schematic display of the magnetic field gradient. The magnetic moment of the ions interacts with field gradient resulting in a shorter flight time.

The RF quadrupole excitation is applied with the different frequencies near the calculated value of the cyclotron frequency. In a resonant case, when frequency of the quadrupole field matches with the cyclotron frequency of ion, the magnetron motion is completely converted into the modified cyclotron motion. Therefore, energy of radial motion is maximal and the time-of-flight of ions to the detector is minimal. One obtains the cyclotron frequency of ions in the minimum of resonance curve by fitting a theoretical line-shape. Fig.2.18 shows an example of a TOF-ICR scan with the fitted function.
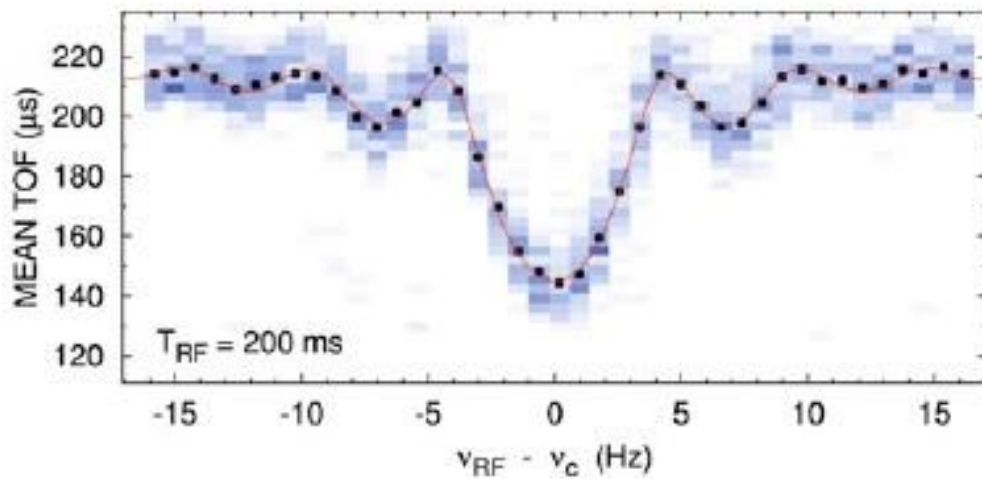
Fig. 2.18: A time-of-flight ion-cyclotron resonance curve for ^{54}Co ions using an excitation time of 200 ms. Black dots show the average TOF plotted as a function of excitation frequency. Shadowed boxes show the density of detected ions and red line is the theoretical fit function to the measured data.

By measuring the cyclotron frequency the mass can be defined from equation (2.8).

In the experiment the ratio between frequency of the reference ions and the frequency of investigated ions is defined by the formula (2.11).

$$r = \frac{f_{c,ref}}{f_c} \qquad (2.11)$$

The atomic mass of an unknown ion can be determined by equation (2.12)

$$m_{atoms} = \frac{f_{c,ref}}{f_c}\left(m_{ref} - m_e\right) + m_e \qquad (2.12)$$

where $f_{c,ref}$ is the cyclotron frequency of the reference ions, f_c is the cyclotron frequency ions, m_{ref} is the mass of the reference ions, m_e is the electron mass.

3. Experimental methods

3.1 Laser ablation ion source

The laser ablation ion source was placed between the switchyard and the RFQ cooler. Previously the setup was placed into the switchyard chamber, but due to limited space it was decided to move the laser ablation ion source closer to the JYFLTRAP see Fig. 3.1. In order to be able to place this ion source on the new place previous setup [14] was redesigned.

The current setup, which is shown in Fig. 3.2 (c) is built in a DN 100 ISO-K pipe system. This system consists of mounting flange on which the einzel lens is mounted. This flange is attached to the first pipe where all electrical inputs of ion optics are placed. A Linear Motion Feedthrough device coupled to target and motor cell has also been connected to this pipe. The first pipe with the regulating elements is connected to the second pipe that houses also the transparent laser window. The ions generated with this ion source should have a certain kinetic energy to enable us to use the RFQ cooler to improve the ion beam properties. For this purpose the ion source setup was lifted up to 30 kV by a Spellman high voltage DC supply. The whole setup is separated from the rest of the beamline with a DN 100 ISO-F plastic insulator.

COLLINEAR LASER HUT
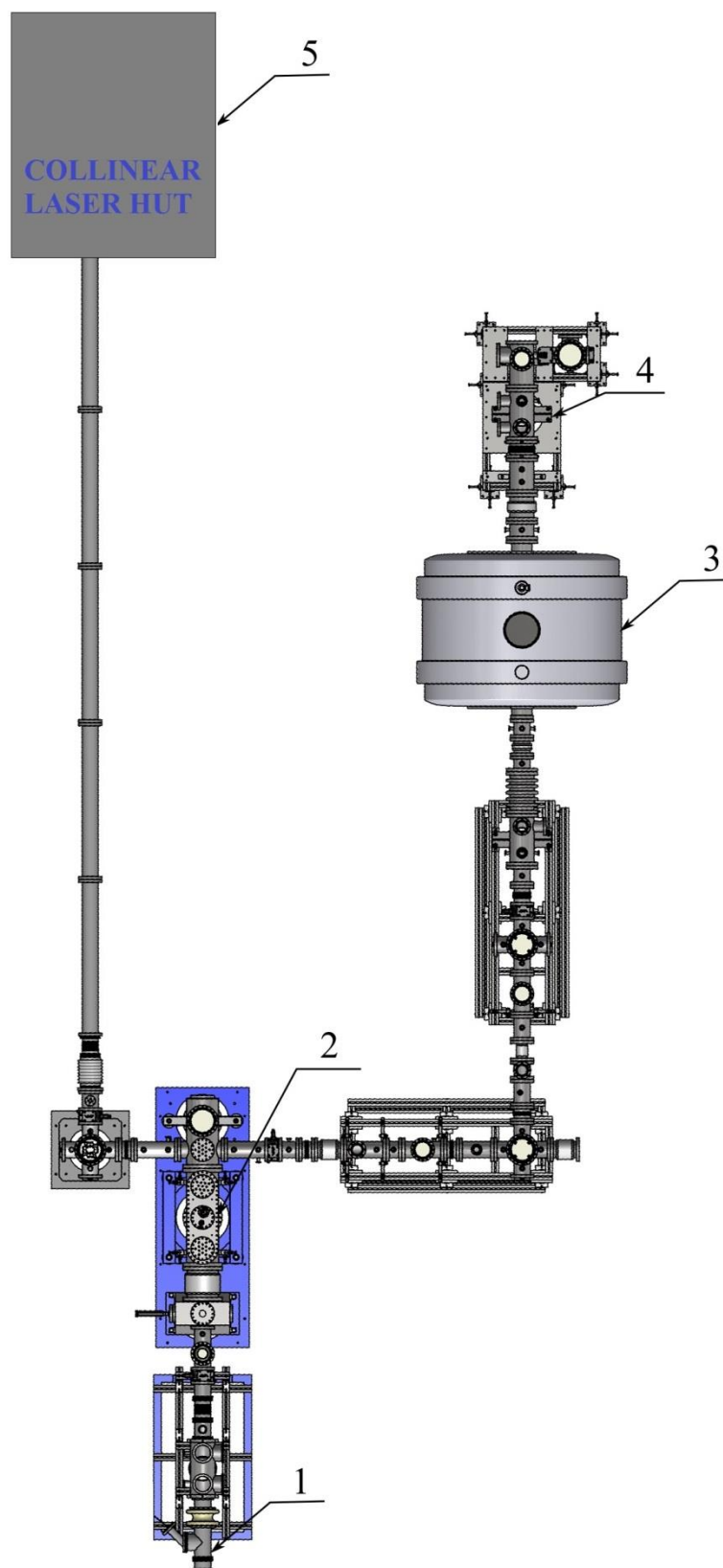
Fig. 3.1: A schematic view of the position of the laser ablation ion source in the IGISOL facility. 1) the laser ablation ion source, 2) RFQ cooler/buncher, 3) JYFLTRAP, 4) MCP position, 5) collinear laser hut.
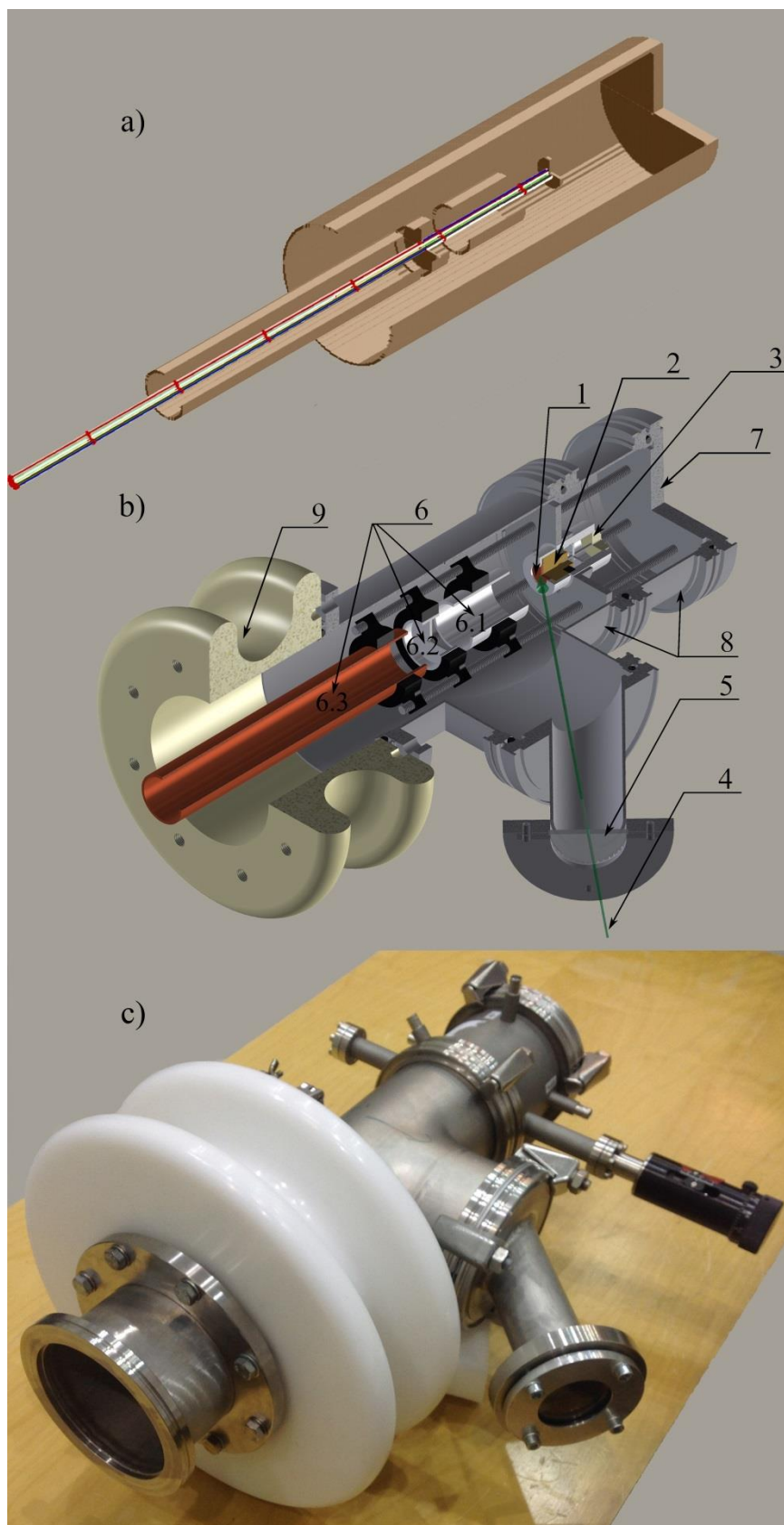
Fig. 3.2: Steps of creation of the laser ablation ion source. From a) simulation of the 3D model of the ion optics in SIMION 8.0 and b) 3D model of the setup where 1) target, 2) target holder, 3) motor, 4) laser beam, 5) window, 6) einzel lens, 7) mounting flange 100 ISO-K with mounting rods, 8) housing pipes DN 100 ISO-K, 9) plastic insulator, to c) the real setup.

The target is placed on a rotating target holder, driven by an electric motor. The motor is used to rotate this target with a constant speed and therefore prevent burning only one area of the target. The target and the motor form a moving cell. One is able to move this cell in and outwards of the pipe center by using a CF16 Linear Motion Feedthrough device. The main purpose of this linear motion is to ablate ions from the certain spot on the surface of the target, which corresponds to the central line of the ion optics. This becomes important when the geometric center of the target is burned and the laser point has to be moved to the peripheral areas of the target. In other words, after obtaining optimal amount of ablated ions per scan and after burning corresponding region on the target, instead of move laser point relatively to the setup and thereby change ion source position relatively to the ion optics, we are moving target. The target and the motor are electrically connected to the body of the setup and thus also lifted to 30kV.

Ion optics that consists of three cylindrical electrodes is placed in front of the target. Optimal voltages, positions and dimensions of the electrodes were simulated in SIMION 8.0, see Fig. 3.2 (a), in order to focus the beam in to the injection electrodes of the RFQ cooler/buncher. Fig. 3.3 shows an illustration of simulation of ions trajectories from the source to the RFQ deceleration electrodes.

After the simulations, good voltages and dimensions for the electrodes were found. These values are present in Table 3.1.

Table 3.1: Electrodes characteristics of the laser ablation ion source, which provide 39% efficiency in the simulations.

Electrode	Voltage, V	Length, mm	Diameter inner/outer, mm
3.1	+29000	50	3/35
3.2	+28000	15	33/35
3.3	+25000	220	33/35
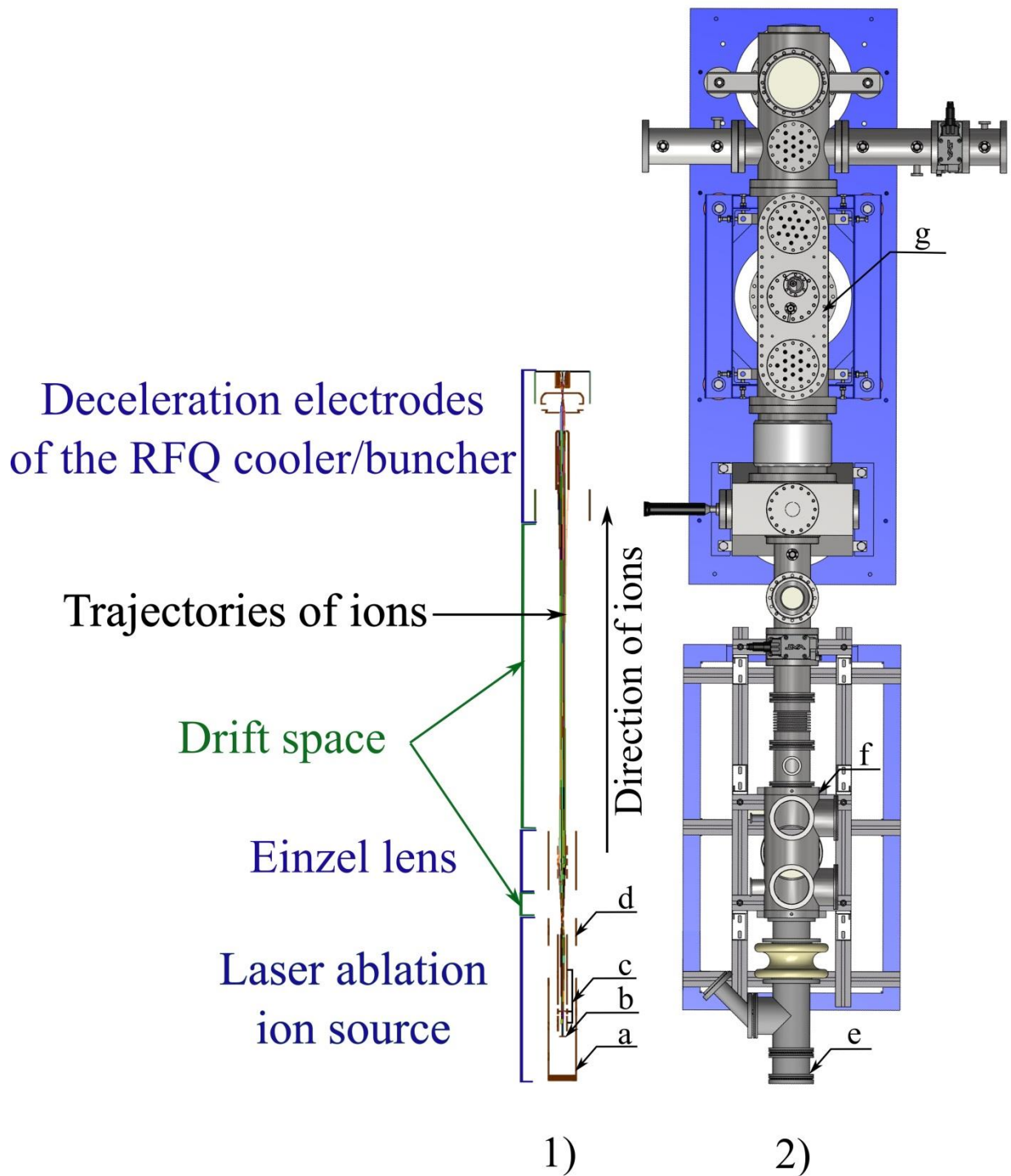
Fig. 3.3: An illustration of the position of the laser ablation ion source relative to the RFQ cooler/buncher in the IGISOL facility. 1) View of simulation in SIMION 8.0 of ions movement from the source to the RFQ deceleration electrodes where a) housing pipes, b) rotation pellet, c) einzel lens of the ion source, d) connection pipe between the ion source and einzel lens in the ground potential. 2) Top view of the 3D model of the beamline including e) the laser ablation ion source, f) einzel lens and g) RFQ cooler/buncher.

As mentioned above each electrode in the einzel lens array has its own voltage. To feed these voltages in addition to the main power supply we have used 3 smaller Spellman power supplies in a high-voltage platform, see Fig. 3.4. Two of them provided up to -3 kV and one up to -5 kV output voltages. After a few test runs of the setup, short circuits were discovered which led to the system failure. After this failure, it was decided to simplify the system and go from three to one power supply.
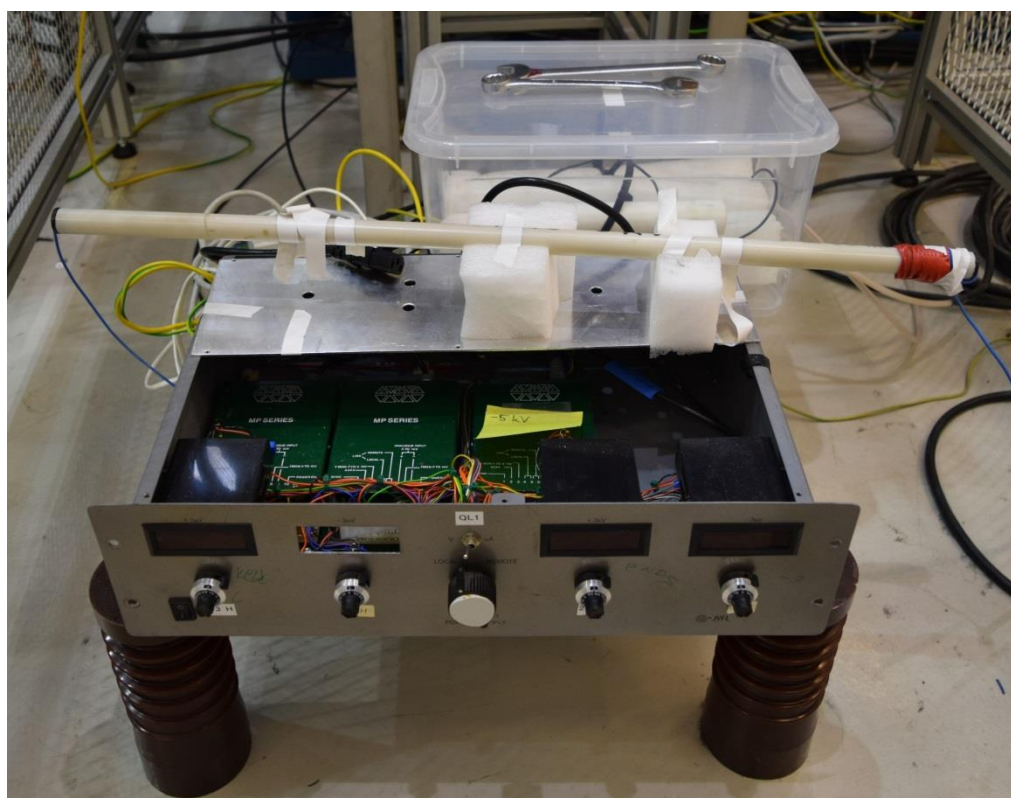
Fig. 3.4: The main power supply for the applying voltage to the einzel lens.

The new modified device required additional simulation. It was enough to keep all electrodes in the same voltage. In this case it was possible to reach 19% efficiency with +26592 V applied to each electrode. This efficiency was enough for the mass measurements.

For producing ions, a target was irradiated by Quantel Brilliant Nd:YAG 532 nm laser, see Fig.3.5. The operation principle of this method is based on generation of plasma by a pulsed laser beam focused on the surface of a target.

[15]. By this technique large amounts of different ions can be obtained in a range of ions with unit charge to the clusters of ions, in addition highly-charged ions [16].
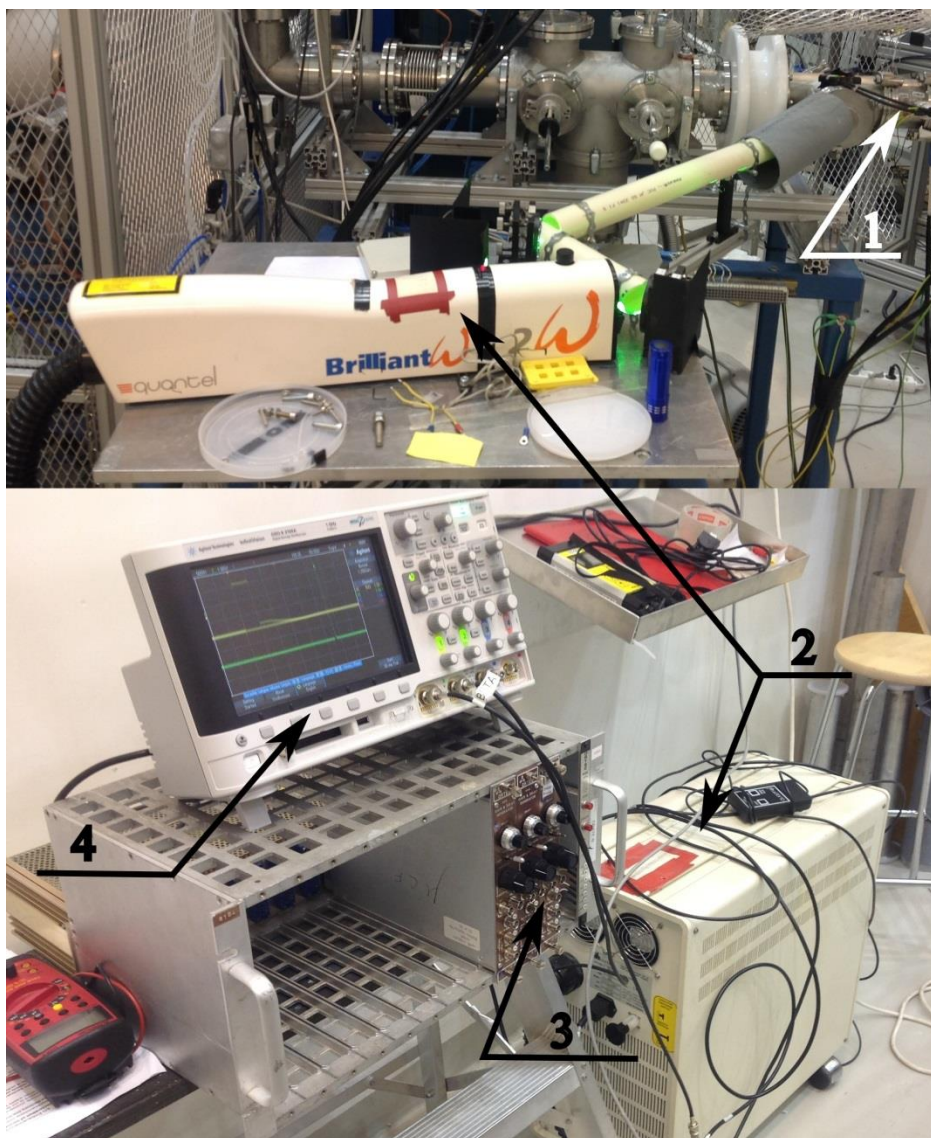
Fig. 3.5: A photo of a system for laser ablation 1) Laser ablation ion source, 2) Quantel Brilliant Nd:YAG 532 nm laser, 3) Ortec 416A Gate and Delay Generators, 4) oscilloscope.

Time interval between the laser pulses was regulated by 3 in series connected Ortec 416A Gate and Delay Generators. The laser power was measured as a function of the delay time with powermeter. Fig. 3.6 shows the result of this measurement. The delay time between the pulses was set in range 240 - 265 µs, which was appropriate for the target ablation. More precisely time intervals were

tuned in such a way to have an optimal amount of counts during the mass measurements.
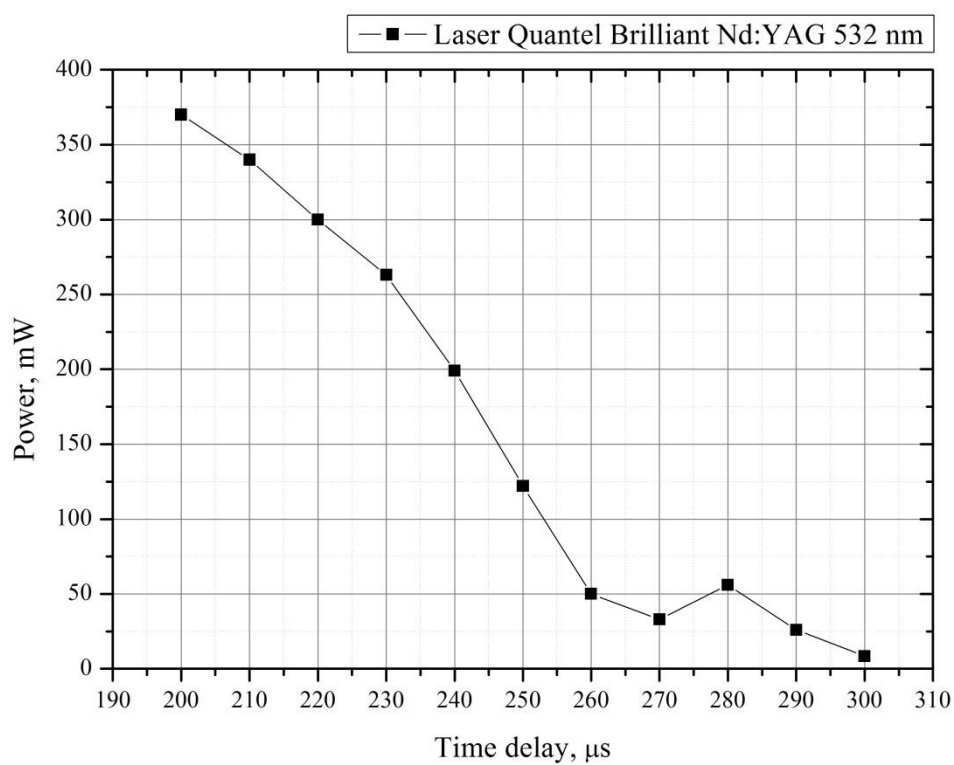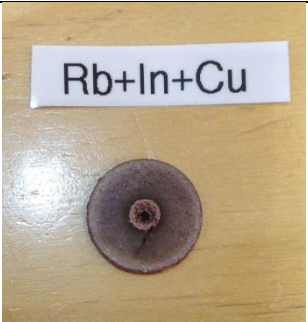
Fig. 3.6: Power of the Quantel Brilliant Nd:YAG 532 nm laser as a function of time delay between flashlamp and Q-switch.

3.2 Targets

At the present ion ablation ion source setup, atoms were obtained by ablation of solid targets with a Quantel Brilliant Nd:YAG 532 nm laser. The targets were divided in to two categories: the first type of targets was used for testing the ion source and the second type of targets was used for cross-reference mass measurements.

Table 3.2: Targets for the test and the cross-reference mass measurements**.**

Target materials		Dimensions (mm)	Target photo
Cu		20x20x0,5	
Sn		20x20x1,7	
Elements	Chemical compounds	d =16 h = 2	
Rb, In, Cu	RbCl, InCl$_2$, Cu		

The testing of the laser ablation ion source did not set strict demands on the target material. The main requirements of first type of targets were simplicity of ion producing and possibility to compare results with an existing electric

discharge ion source. For these reasons copper and tin were used. The photos of targets and their characteristics are in Table 3.2. The targets were cut from thin sheets of metal. The limitations on this target size were established by the target holder and were 20x20 mm square surface shape with thickness which could deviate in range 0,5 – 5 mm.

The second type of the targets was specially manufactured for studying of the systematic effects of JYFLTRAP. For this purposes uncertainty in atomic masses of isotopes which composed target materials should not exceed 10 eV. Suitable isotopes have been chosen from AME2012 [17], see Table 3.3.

Table 3.3: Suitable isotopes for the cross-reference mass measurements.

Elements	Isotopes	Mass excess uncertainty (keV)	Abundance
Ge	^{72}Ge	0,08	27,45%
	^{73}Ge	0,06	7,75%
	^{74}Ge	0,013	36,50%
	^{76}Ge	0,018	7,37%
Se	^{74}Se	0,015	0,89%
	^{76}Se	0,018	9,37%
	^{77}Se	0,06	7,67%
Rb	^{85}Rb	0,005	72,17%
	^{87}Rb	0,006	27,83%
In	^{115}In	0,012	95,71%

The composition of the targets consisted of following chemical compounds: GeO_2, Se, RbCl and $InCl_2$. These compounds were taken as a powder and were compressed into the solid body targets by using a Paul Weber Vacuum Press Tool which is shown in Fig. 3.7. The proportions of the components in the mixture were found from the following calculations, also the fact that we need to

have approximately equal amount of different stable isotope atoms in the target was taken into account.

Fig. 3.7: A photo of the Paul Weber Vacuum Press Tool.

We could approximate the number of isotope atoms refer on a reasonable mass that provide durability of the target. Experimentally we found that the targets stay solid and do not break out under mechanical vibrations, if target mass is in the range of 1,5 − 2 g and the amount of copper powder which was used as a glue, is at least half of the target mass.

Taking the number of isotope atoms $N_{\text{isotope atoms}}$ as fixed value, we could find the number of element atoms $N_{\text{element atoms}}$ in the target referring on the abundance [17]

$$N_{element\ atoms} = \frac{N_{isotope\ atoms}}{Abundance}.$$
(3.1)

Number of chemical compounds N_{comp} is proportional to $N_{element\ atoms}$ in the target and inversely proportional to the proportionate number of atoms of the element in the compound

$$N_{comp} = \frac{N_{element\ atoms}}{n},$$ (3.2)

Where n is the proportionate number of atoms of the element in the compound. The mass of chemical compound is equal to

$$m_{comp} = \frac{M_{comp}}{N_A} \cdot N_{comp},$$ (3.3)

Where M_{comp} is the molar mass of the chemical compound and it is equal to the sum of the molar masses of each constituent element. The molar masses were taken from [18]. N_A is the Avogadro number.

The second type of targets could contain a different combination of two or more chemical elements simultaneously, what was not easy to achieve with electric discharge ion source. This gives a good possibility for studying systematics effects of JYFLTRAP, by using elements with the small mass uncertainty.

4. Measurements

The ions were ablated from a pellet with the Quantel Brilliant Nd:YAG 532 nm laser which operated on 10 Hz repetition frequency and injected into the RFQ cooler/buncher. The RFQ cooler was operated at 613 kHz frequency. In the cooler ions lost part of their energy and subjected to a primary mass-selectivity. Then the cooled ions were transported further to the Penning trap. In the first test measurements time-of-flight of ions between first Penning trap (purification trap) and a microchannel plate (MCP) were measured. To perform these measurements in the purification trap cyclotron and magnetron excitations were turned off and ions were directly extracted to the MCP from the purification trap. The ions were trapped for 300 ms. But opening time of injection potential wall was changed. In the Fig. 4.1 is shown time-of-flight distribution of ions between the trap and the MCP detector, where injection potential wall was opened for 163, 190 and 221μs after extraction of the ions from the RFQ.
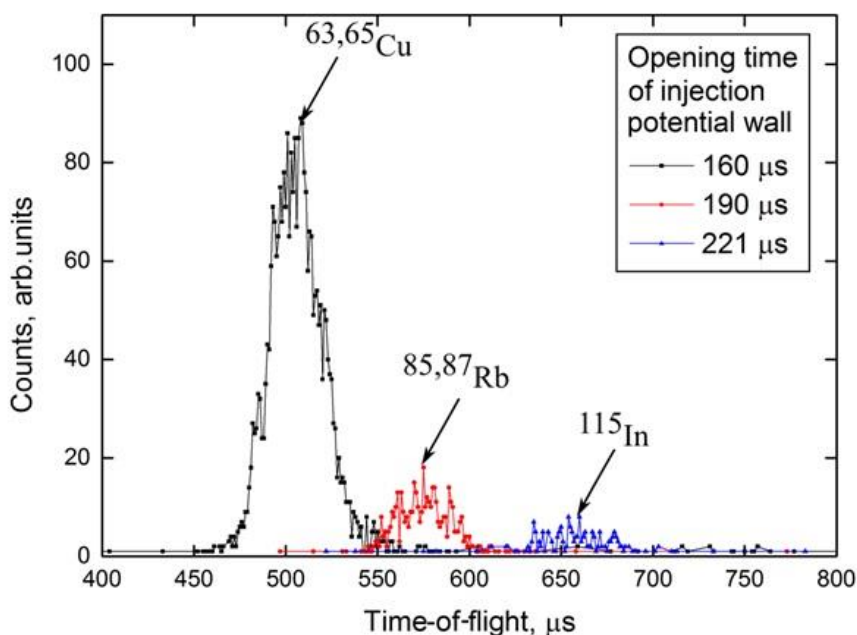
Fig. 4.1: Counts as function of time-of-flight for ions ablated from the compound target. These distributions made for three opening times of injection potential to the first trap 160, 190 and 221 μs. The plot shows three peaks which correspond to masses of five different ions ^{63}Cu, ^{65}Cu, ^{85}Rb, ^{87}Rb and ^{115}In.

The next step was the precise mass measurements. For these measurements the magnetron and cyclotron excitations were on in both purification and precision Penning traps. The first trap was used for isobaric mass-purification [19]. The use of the second trap allows precisely determine the masses of the ions.

The timing patterns for mass measurement for different ions are shown in Fig. 4.2.
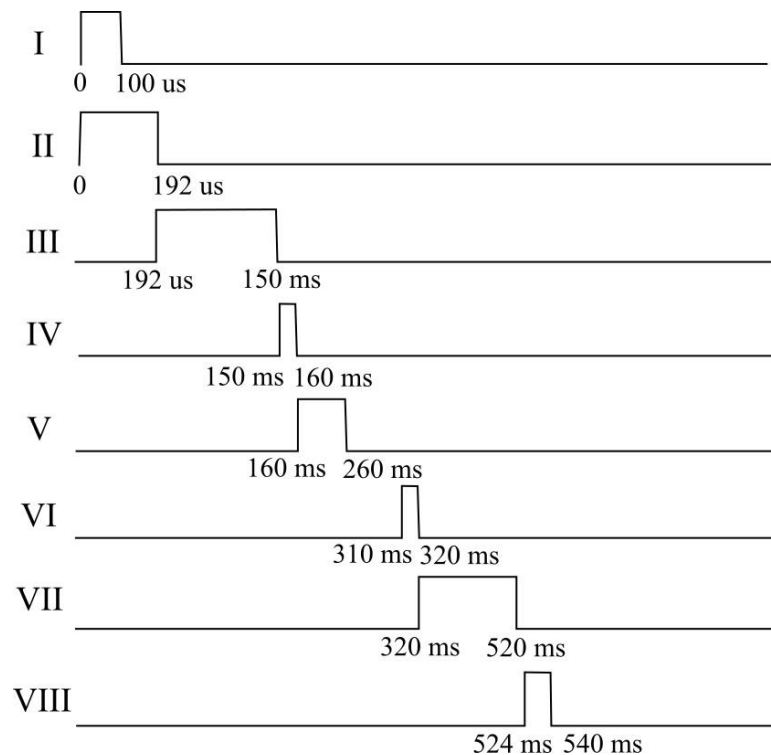
Fig. 4.2: A typical scheme (not in scale) used during a mass measurement. I is cooler extraction, II is the trap wall 1 open (injection), III is an axial cooling, IV is magnetron excitation in the purification trap, V is cyclotron excitation in the purification trap, VI is magnetron excitation in the precision trap, VII is cyclotron excitation in the precision trap, VIII is trap wall 2 open (extraction).

The beam is extracted from the RFQ cooler/buncher as a bunch and it is captured into the first trap. By lowering of the injection wall potential ions fly into the purification trap. Right after that the potential is increased and the ions are trapped. The opening time of the trap depends on the mass of investigated ions. An axial cooling happens before a magnetron excitation is used. The duration of the magnetron excitation was 10 ms at the magnetron frequency $\nu_- =$ 1740 Hz and amplitude A = 400 mV which remove all ions from trap center.

After that during 100 ms the quadrupole excitation with amplitude A = 300 mV transforms the magnetron motion into the modified cyclotron motion and ions are recentered. Then the ions were transported into precision trap, where the magnetron excitation was on about 10 ms with the magnetron frequency $v_- = 170$ Hz and amplitude A = 60 mV and quadrupole excitation was about 200 ms with amplitude A = 56 mV. And finally, ions were extracted to the MCP detector. The total cycle duration is 540 ms.

The examples of time-of-flight resonances as a function of the quadrupolar excitation frequency applied in the precision Penning trap are shown in Figs. 4.3. – 4.6.
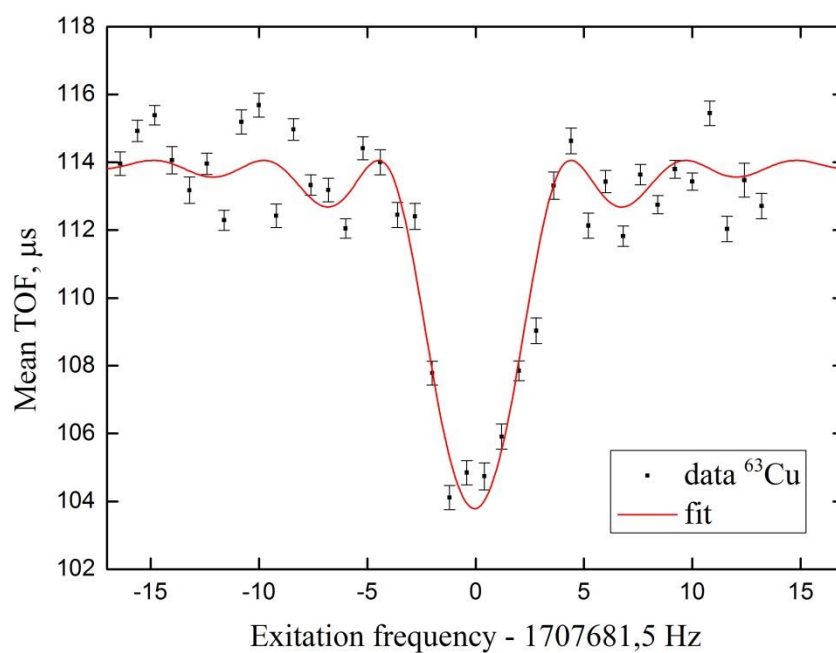
Fig. 4.3: Example of a time-of-flight resonance as a function of the quadrupolar excitation frequency for ^{63}Cu ions. Black dots show the average TOF with its uncertainty and red line is the theoretical fit function to the measured data.
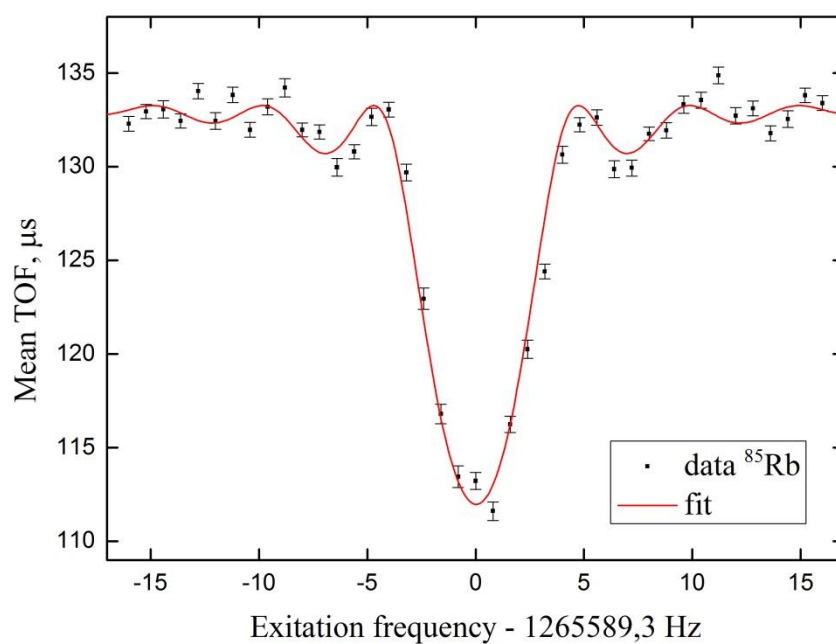
Fig. 4.4: Example of a time-of-flight resonance as a function of the quadrupolar excitation frequency for ^{85}Rb ions. Black dots show the average TOF with its uncertainty and red line is the theoretical fit function to the measured data.
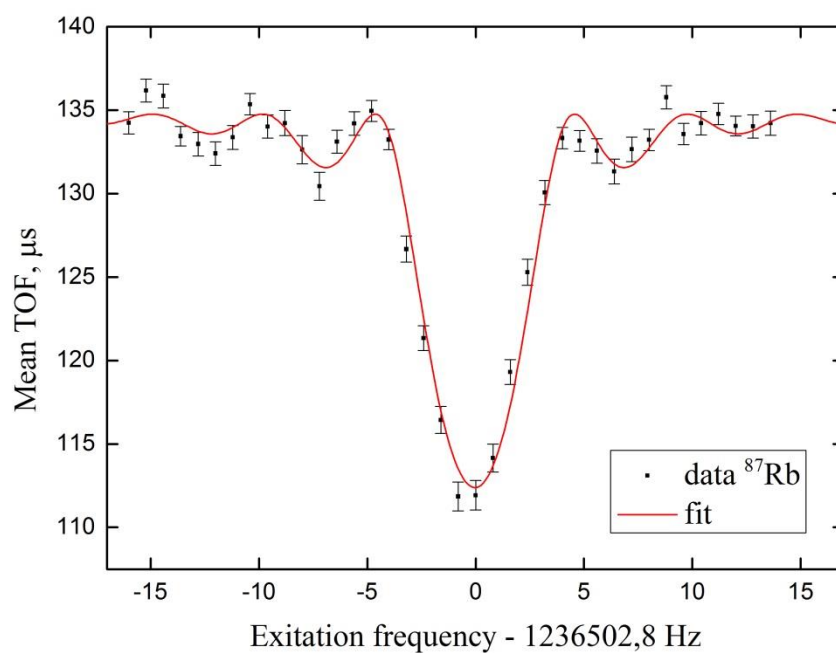
Fig. 4.5: Example of a time-of-flight resonance as a function of the quadrupolar excitation frequency for [87]Rb ions. Black dots show the average TOF with its uncertainty and red line is the theoretical fit function to the measured data.
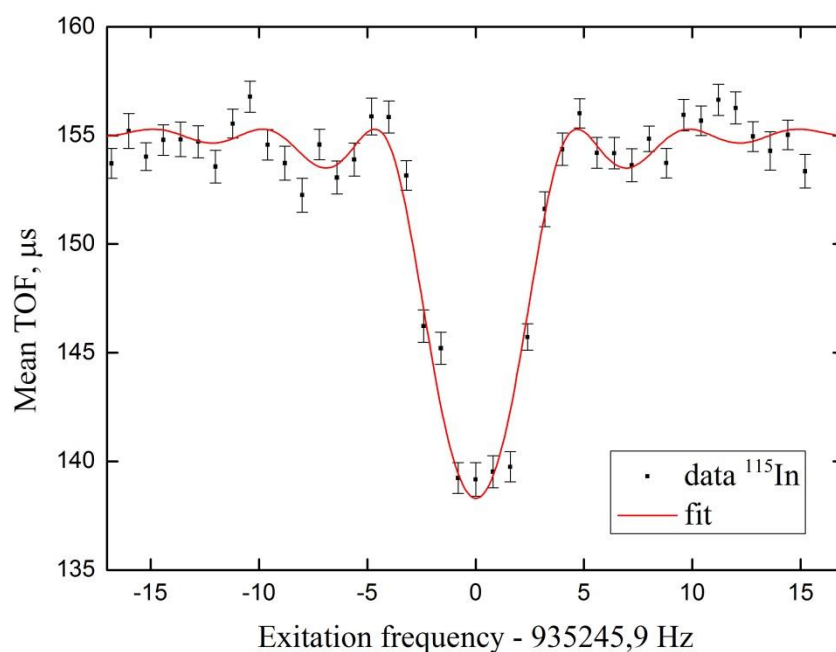
Fig. 4.6: Example of a time-of-flight resonance as a function of the quadrupolar excitation frequency for [115]In ions. Black dots show the average TOF with its uncertainty and red line is the theoretical fit function to the measured data.

5. Conclusions

In this work the laser ablation ion source was redesigned and modified for the IGISOL-4 facility. The ion source showed good ion transmission efficiency and flexibility for the target materials that might be used in this source.

The compound targets which were specially designed for the cross-reference mass measurements at JYFLTRAP were tested and they showed a long lifetime. The lifetime of these targets plays a role in the cross-reference mass measurements, which can last several hours. The measurements that will be performed with this ion source will help to reveal such systematics effects of the JYFLTRAP as the long-term linear drift in the magnetic field, mass-dependent uncertainty and residual uncertainties. However, these studies would be already Ph. D level studies and therefore they are not part of this thesis. Nevertheless, one can calculate the magnetic field B from the TOF-ICR resonances that are shown in Figs. 4.3 − 4.6 and it equals B = 7,001782071±0.0000117 T.

6. References

1.   V. S. Kolhinen et al., Nucl. Instrum Methods Phys. Res., Sec. A 528 (2004) 776.

2.   T. Eronen et al., Eur. Phys. J. A 48 (2012) 46.

3.   J. Äystö, Nucl. Phys. A 693 (2001) 477.

4.   Nieminen et al., Nucl. Instrum Methods Phys. Res., Sec. A 469 (2001) 244.

5.   G. Savard et al., Phys. Lett. A 158 (1991) 247.

6.   Heikkinen P. European Cyclotron Progress Meeting (ECPM XXXVII), Groningen, The Netherlands, 2009, p. 37.

7.   I.D. Moore et al., Nucl. Instrum Methods Phys. Res., Sec. B 317 (2013) 208–213.

8.   I.D. Moore et al., Hyperfine interactions 223 (2014) 17-62.

9.   H.J. Xu et al., Nucl. Instrum. Methods Phys. Res., Sec. A 333 (1993) 274.

10.   P. Karvonen et al., Nucl. Instrum. Method Phys. Res., Sec. B 266 (2008) 4797-4807.

11.   L. S. Brown, G. Gabrielse, Rev. Mod. Phys. 58 (1986) 233.

12.   V.S. Kolhinen et al., Nuclr. Instrum. Methods Phys. Res., Sec. B 317 (2013) 506-509.

13.   M. König et al., Int. J. Mass Spectr. Ion. Proc. 142 (1995) 95.

14.   V.-V. Elomaa et. al., Nucl. Instrum. Methods Phys. Res., Sec. B 266 (2008) 4425–4428.

15.   Bernhard Wolf, Handbook of Ion Sources, (1995) 149.

16.   K. Blaum, Anal. Bioanal. Chem, 377 (2003) 113.

17.   M. Wang, G. Audi et.al., The Ame2012 atomic mass evaluation (II) Tables, graphs and references, CPC(HEP&NP), (2012) 36(12) 1603-2014.

18.   M.E. Wieser, Pure Appl. Chem., Vol. 78, No. 11, (2006) 2051–2066.

19.   H. Raimbault-Hartmann et al., Nucl. Instrum. Methods Phys. Res., Sec. B 126 (1997) 378.

Acknowledgments

I would like to thank Prof. Ari Jokinen for the given possibility to work on my Master's thesis in the IGISOL group. I would like to express my deepest appreciation to my supervisor Dr. Veli Kolhinen for help in all stages of my Master's project, for his professional advices in experimental work. Also, I would like to thank all members of the IGISOL group for the warm welcome and friendly environment.

I also warmly grateful to my husband Oleksii Poleshchuk for his help and support.

Finally, I thank my mother for encouragement and love.

Appendices

A. SIMION simulation

The following geometry file code, which reproduces the structure of the laser ablation ion source electrodes, was used in the SIMION simulations.

```
;Kateryna Poleshchuk
; C-cluster 10.06.2014
PA_define (600,52,1,c,y,e)
; tekee 3D x ja y symmetriat
Locate(0,0,0,1,90,0,0);origo kuvalle
 {
;------------------------------------------------------------
Electrode(1)
 ;gnd electrode
{


  Fill
        {
         within{cylinder(0,0,348,50,50,348)}
         notin{cylinder(0,0,348,48,48,335)}


        }
   }
;------------------------------------------------------------
Electrode(2)
 ;gnd electrode
{


  Fill
        {
         within{cylinder(0,0,145,10,10,2)}


        }
   }
;------------------------------------------------------------
Electrode(3)
 ;gnd electrode
{


  Fill
        {
         within{cylinder(0,0,212,17,17,50)}
```

```
                notin{cylinder(0,0,212,15,15,50)}


              }
        }
;-------------------------------------------------------
Electrode(4)
 ;gnd electrode
{


   Fill
          {
           within{cylinder(0,0,237,17,17,15)}
           notin{cylinder(0,0,237,15,15,6)}
           notin{cylinder(0,0,228,15,15,6)}
           notin{cylinder(0,0,237,2,2,15)}
          }
     }
;-------------------------------------------------------
Electrode(5)
 ;gnd electrode
{


   Fill
          {
           within{cylinder(0,0,473,17,17,220)}
           notin{cylinder(0,0,473,15,15,220)}


          }
     }
;-------------------------------------------------------
Electrode(6)
 ;gnd electrode
{


   Fill
          {
           within{cylinder(0,0,518,50,50,75)}
           notin{cylinder(0,0,518,48,48,75)}


          }
     }
;-------------------------------------------------------
;-------------------------------------------------------
}
```

B. Operating voltages

Tables B.1 – B.6 contain voltage values that were used during the measurements with the laser ablation ion source. The voltages order in the tables is following the beam direction from the RFQ cooler/buncher to the MCP detector.

Table B.1: Operating voltages of RFQ cooler/buncher electrodes.

	U, V
DE1	3260
DE2	2810
V_{acc}	800
EE1	145
QPL1	447
QPR1	997
QPS4	2143
QPL2	700

Table B.2: Operating voltages for optics in beamline from RFQ cooler/buncher to the bender.

	U, V
STQ2 X	822,399
STQ2 Y	838,50
STQ3 X	812,20
STQ3 Y	827,70
FocQ1	413,69
STQ4 up	900,20
STQ4 right	854,70
STQ5 up	854,10
STQ5 right	857,50
STQ6 up	562,20
FocQ2	859,29
STQ6 right	847,00
STQ7 right	892,89
STQ7 down	887,29

Table B.3: Typical operating voltages used for the bender.

	U, V
Bender 1	1555
Bender 2	602
Bender 3	1095
Bender 4	2525

Table B.4: Operating voltages used for optics in the beamline from the bender to the trap.

	U, V
STQ8 up	865,20
STQ8 right	881,39
STQ8 down	891,50
FocQ3	684,10
FocQ4	638,10
STQ9 up	856,89
STQ9 right	853,20
STQ10 up	841,70
STQ10 right	861,79
STQ11 up	859,29
STQ11 right	878,39
FocQ5	630,29

Table B. 5: Operational voltages of Penning traps electrodes

		ISEG channel	U, V
Injection			
Inj. 1 – Inj. 10		ISEG 1.0	329,00
Inj. 11 – Inj. 12		ISEG 1.1	100,00
Diaphragm 3 mm		ISEG 1.2	100,00
Purification trap			
End-cap electrodes 2 – 3	Open	ISEG 1.3	100,00
	Closed	ISEG 1.4	0,1
End-cap electrode 1	Open	ISEG 1.5	100,00
	Closed	ISEG 1.6	0,01
Correction ring electrode 2	Open	ISEG 1.7	100,00
	Closed	ISEG 1.8	34,00

Correction ring electrode 1	Open	ISEG 1.9	100,00
	Closed	ISEG 1.10	83,00
Ring electrode (dipole)		ISEG 1.11	102,19
Ring electrode (quadrupole)		ISEG 1.12	100,00
Ring electrode free segments		ISEG 1.13	100,00
Correction ring electrode 1	Open	ISEG 1.14	105,00
	Closed	ISEG 1.15	83,00
Correction ring electrode 2	Open	ISEG 2.0	105,00
	Closed	ISEG 2.1	34,00
End-cap electrode 1 – 3	Open	ISEG 2.2	105,00
	Closed	ISEG 2.3	0,1
Precision trap			
End-cap electrode	Open	ISEG 3.0	105,00
	Closed	ISEG 3.3	85,83
Correction ring electrode 2	Open	ISEG 3.0	105,00
	Closed	ISEG 3.2	89,179
Correction ring electrode 1	Open	ISEG 3.0	105,00
	Closed	ISEG 3.1	94,079
Ring electrode		ISEG 6.2	96,29
Correction ring electrode 1	Open	ISEG 3.4	103,00
	Closed	ISEG 6.0	94,109
Correction ring electrode 2	Open	ISEG 3.4	103,00
	Closed	ISEG 3.6	89,18
End-cap electrode	Open	ISEG 3.4	103,00
	Closed	ISEG 6.1	85,69
Extraction			
Drift 1		ISEG 2.5	104,00
Drift 2		ISEG 2.6	105,00
Drift 3		ISEG 6.7	106,00
Extraction 1		ISEG 2.8	179,00
Extraction 2		ISEG 2.9	249,00

Table B.6: Operating voltages for extraction line ion optics.

	U, V
Extraction electrode	1400
Line	854
STQ8 down	891,50
FocQ7	14700
STQ12 X	390
STQ12 Y	330
FocQ8	6819,99
STQ13 X	50
STQ13 Y	106